IRIS AperTO

UNIVERSITÀ DEGLI STUDI DI TORINO

AperTO - Archivio Istituzionale Open Access dell'Università di Torino

Disentangling Electronic and Vibrational Effects in the Prediction of Band Shapes for Singlet-Triplet Transitions

This is the author's manuscript

Original Citation:

Availability:

This version is available http://hdl.handle.net/2318/1779103 since 2021-09-13T17:13:12Z

Published version:

DOI:10.1021/acs.jpcc.9b01130

Terms of use:

Open Access

Anyone can freely access the full text of works made available as "Open Access". Works made available under a Creative Commons license can be used according to the terms and conditions of said license. Use of all other works requires consent of the right holder (author or publisher) if not exempted from copyright protection by the applicable law.

(Article begins on next page)

12 October 2024

Disentangling Electronic and Vibrational Effects in the Prediction of Band Shapes for Singlet-Triplet Transitions

Amalia Velardo,[*,†] Raffaele Borrelli,[‡] Amedeo Capobianco,[†] Alessandro Landi,[†] and Andrea Peluso[†]

†*Dipartimento di Chimica e Biologia Adolfo Zambelli, Università di Salerno, Via Giovanni Paolo II, I-84084 Fisciano (SA), Italy*

‡*Dipartimento di Scienze Agrarie, Forestali e Alimentari, Università di Torino, Via Leonardo da Vinci 44, I-10095 Grugliasco (TO), Italy*

E-mail: avelardo@unisa.it

Abstract

The band shape of phosphorescent emission of benzophenone has been computed by using the first order perturbative expansion of singlet and triplet states with the spin orbit coupling operator as perturbation and by evaluating Franck-Condon integrals with an efficient strategy for handling the whole set of vibrational coordinates. The computed band shape compares well with the experimental one, showing that modern computational tools yield reliable spin-orbit couplings to be used for evaluating the rates of singlet-triplet transitions in modern optoelectronic devices.

Introduction

Singlet-triplet transitions are ubiquitous in optoelectronic devices.[1–6] In organic light emitting diodes (OLED), triplet excitons are formed in larger amount than singlet ones and therefore significantly affect the efficiency and the spectral properties of the emitted radiation.[7–19] In bulk heterojunction (BHJ) solar cells, formation of triplet charge-transfer (^{3}CT) excitons on nanosecond timescales has been observed in thin films consisting of blends of polymer donors and fullerene derivative acceptors and the low conversion efficiencies observed for those systems have been tentatively imputed to an efficient charge recombination processes occurring via the lowest energy triplet state.[20–23] However, the formation of triplet excitons via ungeminate electron-hole recombination could also play a beneficial role on the energy conversion efficiency, because they slow down the rates of radiative decay to the ground state, thus promoting charge dissociation, which is predicted to be fast enough to effectively compete with the spin forbidden decay to the ground state.[24] Triplet states are also involved in bimolecular upconversion of noncoherent low intensity light, an important process for converting low energy photons into light adequate for photovoltaics, photocatalysis, and bioimaging.[25–28]

For better assessing the role that triplet states can play in organic devices, the kinetics of radiative and non-radiative processes involving those states have to be investigated. Singlet-

triplet transitions are expected to be sufficiently slow to allow the use of the Fermi Golden rule (FGR) for the calculation of the rate constants;[29,30] within that approximation, the rate constant is given by:

$$k_{i\to f} = \frac{2\pi}{\hbar}|V_{if}|^2 F(\Delta E_{if}, T) \tag{1}$$

where V_{if} is the electronic coupling element between the initial and the final state and $F(\Delta E_{if}, T)$ is the Franck-Condon weighted density of states (FCWD).[24,31–35]

Herein, we will focus on the reliability with which the electronic coupling and the FCWD can be obtained by first principle calculations by computing the band shape of phosphorescent emission of benzophenone, using the sum of state expression of the electric dipole transition moment obtained at the second order of perturbation theory. That is a particularly significant test, inasmuch as it involves the calculation of: *i*) the spin-orbit coupling elements between singlet and triplet states, *ii*) the dipole moment transition strengths, and *iii*) the equilibrium geometries of the excited states.

We will show that within such an approach, the band-shape can be reliably reproduced using a manageable number of excited states. Herein we will expose our analysis based on a methodology which requires the computation of Franck-Condon factors.

Of course, different methodologies for predicting band-shapes are available, such as the nuclear ensemble statistical approach. Illustrative computations of the emission spectra of organic molecules carried out with different methodologies and useful comparisons between Franck-Condon based and statistical approaches can be found in ref 36, where the strengths and the weaknesses of the different methodologies are discussed.

Radiative singlet triplet transitions

According to pioneering work by Henry and Siebrand,[37–39] the band shape of singlet-triplet transitions can be computed by using the wavefunctions of the lowest energy singlet $|S_0'\rangle$ and

triplet $|\mathrm{T}_1'\rangle$ states evaluated at the first order of perturbation theory:[40]

$$|\mathrm{S}_0'\rangle = |\mathrm{S}_0\rangle + \sum_{t\geq 1}\sum_{\alpha=1}^{3} \frac{\langle \mathrm{T}_t^\alpha|\, \hat{H}_{\mathrm{SO}}\, |\mathrm{S}_0\rangle}{\mathrm{E}(\mathrm{S}_0)-\mathrm{E}(\mathrm{T}_t)} \cdot |\mathrm{T}_t^\alpha\rangle\,, \tag{2}$$

$$|\mathrm{T}_1'^\alpha\rangle = |\mathrm{T}_1^\alpha\rangle + \sum_{s\geq 0} \frac{\langle \mathrm{S}_s|\, \hat{H}_{\mathrm{SO}}\, |\mathrm{T}_1^\alpha\rangle}{\mathrm{E}(\mathrm{T}_1)-\mathrm{E}(\mathrm{S}_s)} \cdot |\mathrm{S}_s\rangle\,, \tag{3}$$

where $\hat{H}_{\mathrm{SO}}$ represents the spin-orbit coupling operator; $|\mathrm{S}_0\rangle$ and $|\mathrm{T}_1\rangle$ are the unperturbed states and the superscript α denotes the spin states of triplet levels.

By using eqn.s 2 and 3 and recalling that the $\hat{\boldsymbol{\mu}}$ operator cannot remove the orthogonality of T_n^α and T_m^β $(n \neq m)$ when $\alpha \neq \beta$, the electric dipole transition moment of the $\mathrm{T}_1 \rightarrow \mathrm{S}_0$ radiative transition is given by:[37,41,42]

$$\langle \mathrm{T}_1'^\alpha|\, \hat{\mu}_\gamma\, |\mathrm{S}_0'\rangle = \sum_s \frac{\langle \mathrm{T}_1^\alpha|\, \hat{H}_{\mathrm{SO}}\, |\mathrm{S}_s\rangle\, \langle \mathrm{S}_s|\, \hat{\mu}_\gamma\, |\mathrm{S}_0\rangle}{\mathrm{E}(\mathrm{T}_1)-\mathrm{E}(\mathrm{S}_s)} + \sum_t \frac{\langle \mathrm{T}_1^\alpha|\, \hat{\mu}_\gamma\, |\mathrm{T}_t^\alpha\rangle\, \langle \mathrm{T}_t^\alpha|\, \hat{H}_{\mathrm{SO}}\, |\mathrm{S}_0\rangle}{\mathrm{E}(\mathrm{S}_0)-\mathrm{E}(\mathrm{T}_t)}, \tag{4}$$

where $\gamma \in x, y, z$.

Introducing the Born Oppenheimer approximation:[43]

$$|\mathrm{X}_n\rangle \equiv |X_{n,\mathbf{w}}\rangle = |X_n\rangle \otimes |\mathbf{w}\rangle\,; \qquad \mathrm{E}(\mathrm{X}_n) = E_{X_n} + \epsilon_{\mathbf{w}},$$

where $X = S$ or T, $\mathbf{w}$ is the vector collecting the vibrational states of X_n, E and ϵ denote the electronic and vibrational energy, eqn 4 can be cast in the form:

$$\left\langle T_{1,\mathbf{u}}'^\alpha\right|\, \hat{\mu}_\gamma\, \left|S_{0,\mathbf{v}}'\right\rangle = \sum_{s,\boldsymbol{\sigma}} \frac{\langle T_1^\alpha|\, \hat{H}_{\mathrm{SO}}\, |S_s\rangle\, \langle S_s|\, \hat{\mu}_\gamma\, |S_0\rangle\, \langle \mathbf{u}|\boldsymbol{\sigma}\rangle\langle \boldsymbol{\sigma}|\mathbf{v}\rangle}{E_{T_1}+\epsilon_{\mathbf{u}}-E_{S_s}-\epsilon_{\boldsymbol{\sigma}}} + \sum_{t,\boldsymbol{\tau}} \frac{\langle T_1^\alpha|\, \hat{\mu}_\gamma\, |T_t^\alpha\rangle\, \langle T_t^\alpha|\, \hat{H}_{\mathrm{SO}}\, |S_0\rangle\, \langle \mathbf{u}|\boldsymbol{\tau}\rangle\langle \boldsymbol{\tau}|\mathbf{v}\rangle}{E_{S_0}+\epsilon_{\mathbf{v}}-E_{T_t}-\epsilon_{\boldsymbol{\tau}}}, \tag{5}$$

where $\langle X_n|\, \hat{\mu}_\gamma\, |X_m\rangle$ and $\langle X_n|\, \hat{H}_{\mathrm{SO}}\, |X_m\rangle$ imply integration only over electronic coordinates, and $\mathbf{u}$, $\mathbf{v}$, $\boldsymbol{\sigma}$ and $\boldsymbol{\tau}$ are the vectors of the vibrational states of T_1, S_0, and the intermediary

S_s and T_t states, respectively. The possible dependence of $\hat{H}_{SO}$ on the nuclear coordinates and non-Condon effects have been neglected in eq. 5, see next section.

The spectral band shape for radiative triplet-singlet emission is given by:[44,45]

$$I_{TS} = \frac{16\,\mathcal{N}_A \pi^3}{3\,\varepsilon_0 c^3} \sum_{\mathbf{v}} \sum_{\mathbf{u}} \frac{e^{-\beta\epsilon_{\mathbf{u}}}}{Z} |\boldsymbol{\mu}(T'_{1,\mathbf{u}} \to S'_{0,\mathbf{v}})|^2 \int \nu^4 \delta\left(E_{T'_1,\mathbf{u}} - E_{S'_0,\mathbf{v}} - h\nu\right) d(h\nu) \qquad (6)$$

where I_{TS} is the intensity of the transition, i.e. the energy emitted by one mole per second, $\mathcal{N}_A$ denotes the Avogadro number, ε_0 the vacuum permittivity, c the speed of light; Z is the vibrational partition function of the initial state, $\beta = (k_B T)^{-1}$, k_B being the Boltzmann constant, and $|\boldsymbol{\mu}(T'_{1,\mathbf{u}} \to S'_{0,\mathbf{v}})|^2 = \sum_{\alpha} \sum_{\gamma} |\left\langle T'^{\alpha}_{1,\mathbf{u}} \right| \hat{\mu}_\gamma \left| S'_{0,\mathbf{v}} \right\rangle|^2$.

Computational details

All electronic computations have been carried out at the density functional level of theory (DFT) by using the B3LYP potential.[46,47] That level of computations should provide reliable results, according to previous work.[48–50] Geometry optimizations and computations of normal coordinates and harmonic vibrational frequencies were carried out by using the Gaussian package (G09).[51] Spin-orbit coupling elements, vertical excitation energies and transition dipole moments were calculated by using the Amsterdam density functional (ADF) suite of programs.[52,53] Relativistic effects were included in ADF computations through the zeroth order regular approximation (ZORA).[54] Time dependent DFT (TDDFT) was employed for treating all excited states, including T_1. With both G09 and ADF programs, excited states were computed by using a reference closed shell (singlet) ground state. Only for the evaluation of $\langle T^{\alpha}_1 | \hat{\mu}_\gamma | T^{\alpha}_t \rangle$ transition dipole moments we had to resort to the unrestricted formalism. By using $\langle S^2 \rangle$ as an indicator of spin contamination, our calculations yield 2.058 for T_2 state and 2.037 for T_3 state. Therefore, according to Ipatov et al., spin contamination would not severely undermine the quality of our results.[55]

The TZ2P basis set composed of Slater type orbitals was used in the computations with

the ADF program. Because G09 makes use of Gaussian type functions, a perfect match for the results of the two softwares is not attainable. However, we have tested several Gaussian basis sets and found that G09/TZVP gives the closest agreement with ADF/TZ2P. The RMSD between the equilibrium geometries amounts to ca 0.01 Å for both S_0 and T_1 states.

Multidimensional Franck Condon (FC) factors have been computed by using the basis of normal coordinates and the Duschinsky transformation:

$$\mathbf{Q}' = \mathbf{J}\mathbf{Q} + \mathbf{K}, \tag{7}$$

where $\mathbf{Q}$ and $\mathbf{Q}'$ are the normal coordinates of the electronic states involved in the transition, and $\mathbf{J}$ and $\mathbf{K}$ are the rotation matrix and the equilibrium displacement vector, respectively.[56,57]

Equilibrium position displacements and frequency shifts were included in calculations, whereas normal mode mixing effects were neglected, in order to permit an easier storage of a large number of FC integrals.[58] FC factors were computed by using a development version of the MolFC package.[59] The phase of the electronic spin-orbit coupling (SOC) and transition dipole moments appearing in the two summations of Eq.n 5 has been fixed by computing each element of one of the sums in a single run and then using standard algorithms for fixing the phase of the two contributions.[60]

Comparison between the predicted and the experimental band shapes was carried out by: *i*) extracting I_{TS} from experimental spectrum, and *ii*) making coincident the predicted and the experimental shortest wavelength peaks. The usefulness of that procedure has been detailed in ref 61. Predicted intensities have been scaled by a suitable factor, chosen to help the eye in the comparison with the experimental spectrum.

Results and Discussion

In order to identify the excited states which mostly contribute to the spectral band shape, we started by computing excitation energies, transition dipole moments, and spin-orbit couplings (SOC) for the first twenty excited singlet and triplet states of benzophenone at the equilibrium geometry of T_1. The results are reported in Tables 1 and 2, which show that the largest contributions to the spectral band shape of benzophenone phosphorescent emission are provided by a few low energy lying excited states, in particular S_1, S_2, S_5, T_1, and T_2. Taking into account contributions of the first five excited singlets and of T_2 in eq. 5 should provide a reliable approximation to the spectral band shape (see also Figure S6 in the Supporting Information). We have thus focused attention only on those states, for which full geometry optimizations and normal modes calculations have been carried out. For all the excited states but T_2, the computed Hessian matrices exhibit $3N - 6$ positive eigenvalues, confirming that optimizations yielded minimum energy structures; for T_2 the computed Hessian matrix exhibits only one negative eigenvalue, corresponding to asymmetric stretching of C(carbonyl)-C bonds. Since all the attempts to recover a real minimum failed, we have used for that state the CAM-B3LYP functional,[62] which furnished reliable results both for ground- and excited-state equilibrium geometries for aromatic dyes with high dipole moments.[49,61,63]

Inspection of Tables 1 and 2 shows that the predicted transition dipole moment for the S_0-S_1 transition is considerably lower than those for S_0-S_3 and S_0-S_4, in excellent agreement with the experimental absorption spectrum, thus testifying the reliability of B3LYP in predicting dipole transition moments. Moreover computations agree with the experimental spectrum which shows that the longest wavelength absorption, peaked at $\approx$ 350 nm, is ca two order of magnitude less intense than the shorter one, peaked at ca 250 nm.[64,65]

Although the S_1-S_0 electric dipole transition moment is small, computations predict a large SOC between S_1 and T_1, so that S_1 will significantly contribute to the spectral band shape. The analysis of the Kohn-Sham orbitals shows that S_1 is a $^1(n, \pi^*)$ state, whereas T_1 is to a larger extent a $^3(n, \pi^*)$ state with a smaller component of $^3(\pi, \pi^*)$,[66] thus exhibiting

Table 1: Energies (eV), transition dipole moments ($\mu_\gamma = \langle S_0| \hat{\mu}_\gamma |S_s\rangle$, a.u.), and spin-orbit (SO) coupling elements ($\langle S_s|\hat{H}_{\rm SO}|T_1^\alpha\rangle$, 10^{-5} a.u.) for the first twenty-one singlet states of benzophenone at the equilibrium geometry of T_1. Relative energies are referred to T_1.

s	$\Delta E_{T_1,S_s}$	μ_x	μ_y	μ_z	$\langle S_s\|\hat{H}_{\rm SO}\|T_1^{(1)}\rangle$	$\langle S_s\|\hat{H}_{\rm SO}\|T_1^{(2)}\rangle$	$\langle S_s\|\hat{H}_{\rm SO}\|T_1^{(3)}\rangle$
0	−2.29	0.00	0.00	−1.24	0.00	0.00	27.3 i
1	0.59	0.00	0.00	−0.11	0.00	0.00	10.2 i
2	1.95	0.00	0.00	−0.26	0.00	0.00	4.59 i
3	1.98	0.14	1.28	0.00	−1.03 − 2.26 i	−1.03 − 2.26 i	0.00
4	2.07	0.16	−1.26	0.00	0.65 + 2.76 i	0.65 + 2.76 i	0.00
5	2.21	0.00	0.00	0.74	0.00	0.00	16.8 i
6	2.63	0.00	−0.73	0.00	1.90 + 0.37 i	1.90 − 0.37 i	0.00
7	2.88	0.15	−0.12	0.00	−0.66 + 0.51 i	−0.66 − 0.51 i	0.00
8	3.08	0.00	0.00	−0.34	0.00	0.00	1.08 i
9	3.29	0.05	−0.38	0.00	0.12 + 0.08 i	0.12 − 0.08 i	0.00
10	3.33	0.00	0.00	−0.13	0.00	0.00	−2.00 i
11	3.42	0.10	−0.71	0.00	0.50 + 0.92 i	0.50 − 0.92 i	0.00
12	3.69	0.00	0.00	0.19	0.00	0.00	2.12 i
13	3.70	−0.16	−0.29	0.00	1.20 + 3.48 i	1.20 − 3.48 i	0.00
14	3.72	−0.04	−0.46	0.00	−3.41 − 10.0 i	−3.41 + 10.0 i	0.00
15	3.77	0.00	0.00	−0.12	0.00	0.00	−0.49 i
16	3.84	0.00	0.00	−0.24	0.00	0.00	−8.14 i
17	3.91	−0.08	−0.85	0.00	−0.39 i	0.39 i	0.00
18	3.95	0.00	0.00	0.04	0.00	0.00	2.27 i
19	4.00	0.12	−0.17	0.00	0.10 − 0.37 i	0.10 + 0.37 i	0.00
20	4.22	0.00	0.00	0.14	0.00	0.00	−1.03 i

large SOC couplings with both S_0 and S_1 states, according to El-Sayed's rules.[67] T_2 is a $^3(n,\pi^*)$ state exhibiting a large SOC with S_0. No other triplet states possess large SOC elements with S_0, so that the perturbative sum over triplet states can be safely truncated to T_2.

Equilibrium position displacements of the normal modes of the electronic states which are expected to provide the major contributions to the perturbative summation of Eqn. 5 are reported in Table 3. They have been computed via Duschinsky's transformation of normal modes, using the internal coordinate representation.[33,56,57,68] The equilibrium geometries of S_1 and T_1 states of benzophenone are almost identical, the RMSD between the predicted minimum energy structures amounting to 0.07 Å. That prediction is in line with experimen-

Table 2: Excitation energies (eV), transition dipole moments ($\mu_\gamma = \langle T_1 | \hat{\mu}_\gamma | T_t \rangle$, a.u.), and spin-orbit coupling elements ($\langle S_0 | \hat{H}_{\rm SO} | T_t^\alpha \rangle$, 10^{-5} a.u) for the first twenty excited triplet states of benzophenone at the equilibrium geometry of T_1. Relative energies are referred to S_0.

$\Delta E_{S_0,T_t}$	μ_x	μ_y	μ_z	$\langle S_0 \vert \hat{H}_{\rm SO} \vert T_t^{(1)} \rangle$	$\langle S_0 \vert \hat{H}_{\rm SO} \vert T_t^{(2)} \rangle$	$\langle S_0 \vert \hat{H}_{\rm SO} \vert T_t^{(3)} \rangle$
2.29	0.00	0.00	−0.66	0.00	0.00	27.3 i
2.84	0.00	0.00	0.32	0.00	0.00	14.8 i
3.34	0.02	−0.76	0.00	−1.38 + 0.40 i	−1.38−0.40 i	0.00
3.74	0.00	0.00	0.11	0.00	0.00	1.97 i
3.80	−0.03	−0.17	0.00	0.53+0.09 i	+0.53−0.9 i	0.00
4.33	−0.06	1.61	0.00	0.00	0.00	0.83 i
4.50	−0.09	−0.70	0.00	−1.39 − 0.50 i	−1.39 − 0.50 i	0.00
4.69	0.00	0.00	0.36	2.57 − 3.34 i	−2.57 + 3.34 i	0.00
4.76	0.00	0.00	−0.10	0.00	0.00	1.14 i
4.91	0.02	−0.04	0.00	−0.24−1.93 i	−0.24+1.93 i	0.00
4.94	0.00	0.00	−0.08	0.00	0.00	−0.32 i
5.20	0.00	0.00	0.13	−2.11−2.93 i	−2.11+2.93 i	0.00
5.35	0.00	1.74	0.00	1.72+1.74 i	1.72−1.74 i	0.00
5.39	0.00	0.00	−0.07	0.00	0.00	−0.14 i
5.42	0.00	0.00	0.27	0.00	0.00	2.02 i
5.45	0.18	−0.24	0.00	−1.23+0.42 i	−1.23−0.42 i	0.00
5.53	−0.03	0.30	0.00	0.00	0.00	1.18 i
5.71	−0.01	0.52	0.00	−11.00−0.07 i	−11.00+0.07 i	0.00
6.00	0.00	0.00	0.33	−1.51−0.46 i	−1.51+0.46 i	0.00
6.00	−0.02	−0.54	0.00	0.00	0.00	2.95 i

tal evidence: the sensitized phosphorescence excitation spectra of jet-cooled benzophenone have shown that the $S_1 \leftarrow S_0$ and $T_1 \leftarrow S_0$ spectra are just duplicates of each other in their vibrational structure, clearly indicating that S_1 and T_1 have almost identical minimum energy geometries.[69] The most displaced coordinates for singlet-triplet transitions correspond to low frequency vibrational modes occurring at wavenumbers below 100 cm^{-1}, attributable to in-phase or out-of-phase torsional modes of phenyl rings, and to high frequency vibrational modes occurring at wavenumbers around 1600-1700 cm^{-1}, attributable to in plane stretching and bending modes involving the carbonyl group and adjacent ring carbons, which are responsible for the progression which characterizes the band-shape of the phosphorescence spectrum.

Table 3: Wavenumbers ($\tilde{\nu}$, cm^{-1}) and Equilibrium Position Displacements (K, Dimensionless) of the Most Displaced Normal Coordinates of Benzophenone for the most contributing Singlet and Triplet states.

	$X_n \leftarrow T_1$			$X_n \rightarrow S_0$		
X_n	$\tilde{\nu}_{T_1}$	$\tilde{\nu}_{X_n}$	K	$\tilde{\nu}_{X_n}$	$\tilde{\nu}_{S_0}$	K
S_0	69	61	2.35			
	90	91	0.81			
	1576	1638	0.62			
	1607	1716	-1.88			
S_1	69	61	3.06	68	69	−0.6
	90	99	0.88	1586	1638	0.56
				1629	1716	−1.73
S_2	69	62	2.12	46	42	−1.02
	90	103	1.62	62	61	4.30
	545	537	−0.97	606	654	1.22
	620	562	1.06			
	1591	1581	−0.97			
T_2	69	67	−3.25	67	61	5.40
	90	113	1.65	113	91	−0.81
	280	312	0.82	1537	1617	0.61
	425	430	0.92	1599	1638	0.92
	534	553	−0.77	1653	1716	−2.72
	973	994	0.52			

The theoretical spectrum has been computed using eq.n 6, including in the summations the first five excited singlet states and T_2, limiting the maximum excitation number to three, but for the most displaced modes of Table 3, for which the latter has been set to 20. In order to rationally truncate the infinite summations over the vibrational states appearing in Eqn. 5, which could also cause problems due to accidental degeneracy of vibronic states, we have resorted to the methodology of ref.s 35,70,71. In that approach, the entire Hilbert space H spanned by the vibrational states partitioned as the union of subspaces h_s, in each of which only s simultaneously excited vibrational modes are included, $H = \bigcup_s h_s$.

That partition relies on the fact that usually Franck-Condon integrals significantly decrease as the number of simultaneous excited modes increases, so that contributions to the spectral band shapes of states belonging to h_s subspaces become smaller as s increases, making it possible to efficiently reduce the exponential growing of the size of the computation. Furthermore, the above partition offers also a sort of control of the convergence of the sum of state expression; herein we obtained a satisfying convergence with subspaces up to $s = 4$.

Thermal effects have been considered by Boltzmann-weighting the vibrational excited states originated by the most displaced low frequency modes, namely 69 and 90 cm^{-1} (see Table 3). Those vibrational degrees of freedom have been populated by introducing up to two quanta each, which should be enough at 77 K. Although a few transitions at higher energy than 0-0 are recovered,[72] thermal effects turn out to be rather modest, as shown in Figure S8 of the Supporting Information.

The theoretical and experimental phosphorescence spectra of benzophenone are shown in Figure 1. The spectrum of benzophenone is structured, exhibiting a pronounced vibrational progression pattern at ca 1600 cm^{-1}, which can be associated to carbonyl stretching mode and to other stretching and bending modes which involve the carbonyl group and the bonded ring carbons.

The 0-0 transition predicted upon aligning maximum intensity peaks turns out to be 24 580 cm^{-1}. Rough experimental estimates of the 0-0 frequency are available; $\tilde{\nu}_{00}$ has been

found in ≈ 24200-24500 cm^{-1}, in close agreement with our results.[73,74]

The shape and the width of the theoretical spectrum are in good agreement with their experimental counterpart. The limited number of vibrational states considered in computations prevents from obtaining a continuum spectrum. However, apart from the regions between peaks, where the predicted density of states is low, the whole spectral shape is well reproduced as well as the relative intensity of the main vibrational progression, testifying about the reliability of the computed SOCs and transition dipole moments.

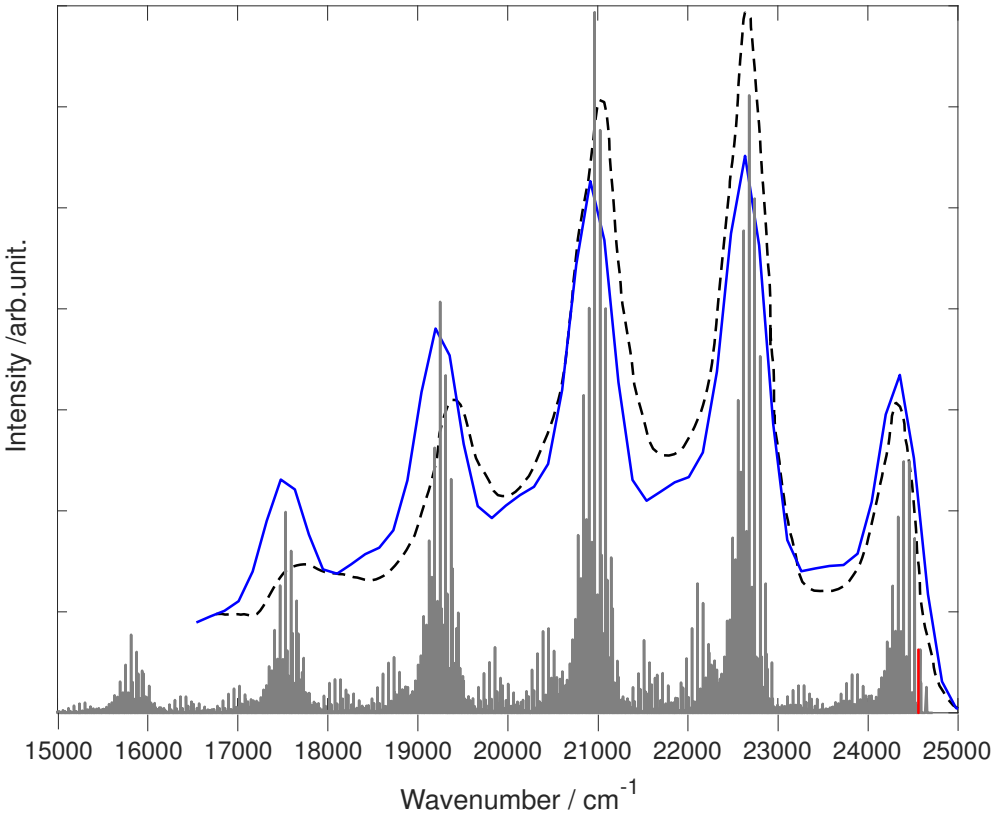

Figure 1: Theoretical (solid gray and blue lines) and experimental (dashed black line) phosphorescence spectra of benzophenone.[73] The assigned 0-0 transition is evidenced in red.

A practical way for considering the whole set of vibrational states is that of approximating vibronic energy differences with the electronic ones. That approximation permits to use the closure relation for the sum over the vibrational states of the intermediate states, leading to:[75]

$$\left\langle T'^{\alpha}_{1,\mathbf{u}} \right| \hat{\mu}_{\gamma} \left| S'_{0,\mathbf{v}} \right\rangle = \Gamma_{S_0,T_1} \langle \mathbf{u} | \mathbf{v} \rangle \tag{8}$$

where:

$$\Gamma_{S_0,T_1} = \sum_s \frac{\langle T_1^\alpha | \hat{H}_{\rm SO} | S_s \rangle \langle S_s | \hat{\mu}_\gamma | S_0 \rangle}{E_{T_1} - E_{S_s}} + \sum_t \frac{\langle T_1^\alpha | \hat{\mu}_\gamma | T_t^\alpha \rangle \langle T_t^\alpha | \hat{H}_{\rm SO} | S_0 \rangle}{E_{S_0} - E_{T_t}}, \tag{9}$$

is a pure electronic factor, and $\langle \mathbf{u} | \mathbf{v} \rangle$ collects the Franck-Condon integrals between the vibrational states of the singlet S_0 and the triplet T_1 states. The latter can now be evaluated by the generating function approach,[45,76,77] according to which the delta function entering Eq. (6) is transformed as:

$$\delta(\Delta E - h\nu) = h^{-1} \int_{-\infty}^{\infty} \exp\left[\mathrm{i} \left(\Delta E - h\nu \right) \tau / h \right] \mathrm{d}\tau, \tag{10}$$

and the integral in (6) can be computed via the transformation:

$$f_{\rm TS}(\tau) = |\Gamma_{\rm TS}|^2 {\rm Tr} \left[\mathrm{e}^{-\mathrm{i}\tau \mathcal{H}_{\rm S}} \mathrm{e}^{(-\beta + \mathrm{i}\tau)\mathcal{H}_{\rm T}} \right]. \tag{11}$$

where $\mathcal{H}_{\rm T}$ and $\mathcal{H}_{\rm S}$ are the vibrational Hamiltonian operators of T_1 and S_0 and τ is a dummy variable: $\tau = t/\hbar$, t having dimensions of time. If $\mathcal{H}_{\rm S}$ and $\mathcal{H}_{\rm T}$ are modeled in harmonic approximation, the trace in (11) can be evaluated into a closed form,[76–78] when the whole Hilbert space of the vibrational states of S_0 and T_1 is considered. The results obtained following this latter approach are also reported in Figure 1.[48] In that case a continuum spectrum is obtained, due both to the completeness of Hilbert space and to the inclusion of hot bands, but the relative intensities of the peaks of the vibrational progression are not very well reproduced, because, as shown by the results of Tables 1 and 2, the replacement of vibronic energy differences with electronic ones is not a good approximation for benzophenone, for which $n\pi^*$ states are strongly coupled to $\pi\pi^*$ states which are close in energy.

We have also analyzed the change of SOC couplings in going from the equilibrium geometry of T_1 to that of S_0 for the three most displaced vibrational coordinates, roughly corresponding to the torsions of the phenyl units and the stretching of the C=O bond. DFT

computations, whose results are summarized in Figures S2-S5 of the Supporting Information, predict very small variations of the SOC for the torsional modes of the phenyl units. Although slightly more consistent variations of the SOCs are found for C=O stretching, the dependence of SOC on nuclear coordinates should affect the phosphorescence spectrum of benzophenone to a very small extent. Indeed, past experience has shown that non-Condon effects become relevant only when SO or dipole moment couplings will vanish.[43,79]

Conclusion

We have shown that the sum over vibronic states expression of singlet-triplet radiative transitions is a viable tool for the computation of spectral band shapes. The excellent agreement between computed and experimental band shape testify that modern computational tools yield reliable electric dipole transition moments and spin orbit couplings. Those quantities, in turn, allow for determining reliable rates of radiative, and non radiative processes which take place in modern technological devices for solar energy conversion and for low power light emitting diodes. The evaluation of these kinetics is a key step toward the design of new organic molecules ensuring better performances.

Acknowledgement

The financial supports of the University of Salerno are gratefully acknowledged. A. V. acknowledges the CINECA award HP10CB456N under the ISCRA initiative, for the availability of high performance computing resources.

References

(1) Baryshnikov, G.; Minaev, B.; Agren, H. Theory and Calculation of the Phosphorescence Phenomenon. *Chem. Rev.* **2017**, *117*, 6500–6537.

(2) Köhler, A.; Bässler, H. Triplet states in organic semiconductors. *Mat. Sci. Engineering: R: Reports* **2009**, *66*, 71–109.

(3) Shao, Y.; Yang, Y. Efficient Organic Heterojunction Photovoltaic Cells Based on Triplet Materials. *Adv. Mater.* **2005**, *17*, 2841–2844.

(4) Arif, M.; Yang, K.; Li, L.; Yu, P.; Guha, S.; Gangopadhyay, S.; Forster, M.; Scherf, U. Harvesting triplet excitons for application in polymer solar cells. *Appl. Phys. Lett.* **2009**, *94*, 063307.

(5) Ostroverkhova, O. Organic Optoelectronic Materials: Mechanisms and Applications. *Chem. Rev.* **2016**, *116*, 13279–13412.

(6) Marian, C. M. Spin-orbit coupling and intersystem crossing in molecules. *WIREs Comput Mol Sci* **2012**, *2*, 187–203.

(7) Baroncini, M.; Bergamini, G.; Ceroni, P. Rigidification or interaction-induced phosphorescence of organic molecules. *Chem. Commun.* **2017**, *53*, 2081–2093.

(8) Botta, A.; Pragliola, S.; Capacchione, C.; Rubino, A.; Liguori, R.; De Girolamo Del Mauro, A.; Venditto, V. Synthesis of poly(4-(N-carbazolyl)methyl styrene)s: Tailoring optical properties through stereoregularity. *Eur. Pol. J.* **2017**, *88*, 246–256.

(9) Minaev, B.; Baryshnikov, G.; Ågren, H. Principles of phosphorescent organic light emitting devices. *Phys. Chem. Chem. Phys.* **2014**, *16*, 1719–1758.

(10) Goushi, K.; Yoshida, K.; Sato, K.; Adachi, C. Organic light-emitting diodes employing efficient reverse intersystem crossing for triplet-to-singlet state conversion. *Nat. Phot.* **2012**, *6*, 253.

(11) Li, X.; Minaev, B.; Ågren, H.; Tian, H. Density Functional Theory Study of Photophysical Properties of Iridium(III) Complexes with Phenylisoquinoline and Phenylpyridine Ligands. *J. Phys. Chem. C* **2011**, *115*, 20724–20731.

(12) Sun, Y.; Giebink, N. C.; Kanno, H.; Ma, B.; Thompson, M. E.; Forrest, S. R. Management of singlet and triplet excitons for efficient white organic light-emitting devices. *Nature* **2006**, *440*, 908.

(13) Baldo, M. A.; Thompson, M. E.; Forrest, S. R. High-Efficiency Fluorescent Organic Light-Emitting Devices Using a Phosphorescent Sensitizer. *Nature* **2000**, *403*, 750–753.

(14) Baldo, M. A.; O'Brien, D. F.; You, Y.; Shoustikov, A.; Sibley, S.; Thompson, M. E.; Forrest, S. R. Highly efficient phosphorescent emission from organic electroluminescent devices. *Nature* **1998**, *395*, 151.

(15) Burroughes, J. H.; Bradley, D. D. C.; Brown, A. R.; Marks, R. N.; Mackay, K.; Friend, R. H.; Burns, P. L.; Holmes, A. B. Light-emitting diodes based on conjugated polymers. *Nature* **1990**, *347*.

(16) Tang, C. W.; VanSlyke, S. A. Organic electroluminescent diodes. *Appl. Phys. Lett.* **1987**, *51*, 913–915.

(17) Helfrich, W.; Schneider, W. G. Recombination Radiation in Anthracene Crystals. *Phys. Rev. Lett.* **1965**, *14*, 229–231.

(18) Pope, M.; Kallmann, H. P.; Magnante, P. Electroluminescence in Organic Crystals. *J. Chem. Phys.* **1963**, *38*, 2042–2043.

(19) Liguori, R.; Botta, A.; Pragliola, S.; Rubino, A.; Venditto, V.; Velardo, A.; Aprano, S.; Maglione, M. G.; Prontera, C.; De Girolamo Del Mauro, A. et al. Study of the electroluminescence of highly stereoregular poly(N-pentenyl-carbazole) for blue and white OLEDs. *Semicond. Sci. Tech.* **2017**, *32*, 065006.

(20) Veldman, D.; Meskers, S. C. J.; Janssen, R. A. J. The Energy of Charge-Transfer States in Electron Donor-Acceptor Blends: Insight into the Energy Losses in Organic Solar Cells. *Adv. Funct. Mater.* **2009**, *19*, 1939–1948.

(21) Piliego, C.; Loi, M. A. Charge Transfer State in Highly Efficient Polymer-Fullerene Bulk Heterojunction Solar Cells. *J. Mater. Chem.* **2012**, *22*, 4141–4150.

(22) Rao, A.; Chow, P. C. Y.; Gélinas, S.; Schlenker, C. W.; Li, C.-Z.; Yip, H.-L.; Jen, A. K.-Y.; Ginger, D. S.; Friend, R. H. The Role of Spin in the Kinetic Control of Recombination in Organic Photovoltaics. *Nature* **2013**, *500*, 435–439.

(23) Chow, P. C. Y.; Albert-Seifried, S.; Gélinas, S.; Friend, R. H. Nanosecond Intersystem Crossing Times in Fullerene Acceptors: Implications for Organic Photovoltaic Diodes. *Adv. Mater.* **2014**, *26*, 4851–4854.

(24) Velardo, A.; Borrelli, R.; Capobianco, A.; La Rocca, M. V.; Peluso, A. First Principle Analysis of Charge Dissociation and Charge Recombination Processes in Organic Solar Cells. *J. Phys. Chem. C* **2015**, *119*, 18870–18876.

(25) Baluschev, S.; Miteva, T.; Yakutkin, V.; Nelles, G.; Yasuda, A.; Wegner, G. Up-Conversion Fluorescence: Noncoherent Excitation by Sunlight. *Phys. Rev. Lett.* **2006**, *97*, 143903.

(26) Ye, C.; Wang, J.; Wang, X.; Ding, P.; Liang, Z.; Tao, X. A new medium for triplet-triplet annihilated upconversion and photocatalytic application. *Phys. Chem. Chem. Phys.* **2016**, *18*, 3430–3437.

(27) Khnayzer, R. S.; Blumhoff, J.; Harrington, J. A.; Haefele, A.; Deng, F.; Castellano, F. N. Upconversion-powered photoelectrochemistry. *Chem. Commun.* **2012**, *48*, 209–211.

(28) Della Sala, P.; Capobianco, A.; Caruso, T.; Talotta, C.; De Rosa, M.; Neri, P.; Peluso, A.; Gaeta, C. An Anthracene-Incorporated [8]Cycloparaphenylene Derivative as an Emitter in Photon Upconversion. *J. Org. Chem.* **2018**, *83*, 220–227.

(29) Landi, A.; Borrelli, R.; Capobianco, A.; Velardo, A.; Peluso, A. Hole Hopping Rates

in Organic Semiconductors: A Second-Order Cumulant Approach. *J. Chem. Theory Comput.* **2018**, *14*, 1594–1601.

(30) Landi, A.; Borrelli, R.; Capobianco, A.; Velardo, A.; Peluso, A. Second-Order Cumulant Approach for the Evaluation of Anisotropic Hole Mobility in Organic Semiconductors. *J. Phys. Chem. C* **2018**, *122*, 25849–25857.

(31) Peng, Q.; Yi, Y.; Shuai, Z.; Shao, J. Toward Quantitative Prediction of Molecular Fluorescence Quantum Efficiency: Role of Duschinsky Rotation. *J. Am. Chem. Soc.* **2007**, *129*, 9333–9339.

(32) Peng, Q.; Yi, Y.; Shuai, Z. Excited state radiationless decay process with Duschinsky rotation effect: Formalism and Implementation. *J. Chem. Phys.* **2007**, *126*, 114302.

(33) Borrelli, R.; Peluso, A. Elementary Electron Transfer Reactions: from Basic Concepts to Recent Computational Advances. *WIREs: Comput. Mol. Sci.* **2013**, *3*, 542–559.

(34) Borrelli, R.; Capobianco, A.; Peluso, A. Hole Hopping Rates in Single Strand Oligonucleotides. *Chem. Phys.* **2014**, *440*, 25–30.

(35) Borrelli, R.; Capobianco, A.; Landi, A.; Peluso, A. Vibronic Couplings and Coherent Electron Transfer in Bridged Systems. *Phys. Chem. Chem. Phys.* **2015**, *17*, 30937–30945.

(36) de Sousa, L. E.; Ribeiro, L. A.; Fonseca, A. L. d. A.; da Silva Filho, D. A. Modeling the Emission Spectra of Organic Molecules: A Competition between Franck-Condon and Nuclear Ensemble Methods. *J. Phys. Chem. A* **2016**, *120*, 5380–5388.

(37) Henry, B. R.; Siebrand, W. Spin-Orbit Coupling in Aromatic Hydrocarbons. Calculation of the Radiative Triplet Lifetimes of Naphtalene, Anthracene, and Phenanthrene. *J. Chem. Phys.* **1969**, *51*, 2396–2405.

(38) Henry, B. R.; Siebrand, W. Spin-Orbit Coupling in Aromatic Hydrocarbons. Analysis of Nonradiative Transitions between Singlet and Triplet States in Benzene and Naphtalene. *J. Chem. Phys.* **1971**, *54*, 1072–1085.

(39) Lawetz, V.; Orlandi, G.; Siebrand, W. Theory of Intersystem Crossing in Aromatic Hydrocarbons. *J. Chem. Phys.* **1972**, *56*, 4058–4072.

(40) McGlynn, S. P.; Azumi, T.; Kinoshita, M. In *Molecular Spectroscopy of the triplet state*; Cliffs, P.-H. E., Ed.; 1969.

(41) Minaev, B.; Ågren, H. The Interpretation of the Wulf Absorption Band of Ozone. *Chem. Phys. Lett.* **1994**, *217*, 531–538.

(42) Minaev, B.; Ågren, H.; De Angelis, F. Theoretical design of phosphorescence parameters for organic electro-luminescence devices based on iridium complexes. *Chem. Phys.* **2009**, *358*, 245–257.

(43) Lin, S. H.; Eyring, H. Study of the Franck-Condon and Herzberg-Teller Approximations. *Proc. Natl. Acad. Sci. U.S.A.* **1974**, *71*, 3802–3804.

(44) Herzberg, G. F. R. S. *Molecular Spectra and Molecular Structure, vol. 1. (Second Edition)*; D. Van Nostrand Company, Inc., 1950, pp 20 and 200.

(45) Lax, M. The Franck-Condon Principle and Its Application to Crystals. *J. Chem. Phys.* **1952**, *20*, 1752–1760.

(46) Becke, A. D. Density-Functional Thermochemistry. III. The Role of Exact Exchange. *J. Chem. Phys.* **1993**, *98*, 5648–5652.

(47) Stephens, P. J.; Devlin, F. J.; Chabalowski, C. F.; Frisch, M. J. Ab Initio Calculation of Vibrational Absorption and Circular Dichroism Spectra Using Density Functional Force Fields. *J. Phys. Chem.* **1994**, *98*, 11623–11627.

(48) Velardo, A.; Borrelli, R.; Peluso, A.; Capobianco, A. First-Principle Calculations of the Band Shapes of Singlet-Triplet Transitions. *J. Phys. Chem. C* **2016**, *120*, 24605–24614.

(49) Capobianco, A.; Esposito, A.; Caruso, T.; Borbone, F.; Carella, A.; Centore, R.; Peluso, A. Tuning Wavefunction Mixing in Push–Pull Molecules: From Neutral to Zwitterionic Compounds. *Eur. J. Org. Chem.* **2012**, 2980–2989.

(50) Capobianco, A.; Carotenuto, M.; Caruso, T.; Peluso, A. The Charge-Transfer Band of an Oxidized Watson-Crick Guanosine-Cytidine Complex. *Angew. Chem. Int. Ed.* **2009**, *48*, 9526–9528.

(51) Frisch, M. J.; Trucks, G. W.; Schlegel, H. B.; *al*, E.-T. Gaussian 09 Revision D.01. Gaussian Inc. Wallingford CT 2009.

(52) te Velde, G.; Bickelhaupt, F. M.; Baerends, E. J.; Fonseca Guerra, C.; van Gisbergen, S. J. A.; Snijders, J. G.; Ziegler, T. Chemistry with ADF. *J. Comput. Chem.* **2001**, *22*, 931–967.

(53) Baerends, E. J.; Ziegler, T.; Atkins, A. J.; Autschbach, J.; Bashford, D.; Baseggio, O.; Bérces, A.; Bickelhaupt, F. M.; Bo, C.; Boerritger, P. M. et al. ADF2017, SCM, Theoretical Chemistry, Vrije Universiteit, Amsterdam, The Netherlands, https://www.scm.com.

(54) van Lenthe, E.; Baerends, E. J.; Snijders, J. G. Relativistic Total Energy Using Regular Approximations. *J. Chem. Phys.* **1994**, *101*, 9783–9792.

(55) Ipatov, A.; Cordova, F.; Joubert Doriol, L.; Casida, M. Excited-state spin-contamination in time-dependent density-functional theory for molecules with open-shell ground states. *J. Mol. Struct. (THEOCHEM)* **2009**, *914*, 60–73.

(56) Peluso, A.; Borrelli, R.; Capobianco, A. Photoelectron Spectrum of Ammonia, a Test Case for the Calculation of Franck–Condon Factors in Molecules Undergoing Large

Geometrical Displacements upon Photoionization. *J. Phys. Chem. A* **2009**, *113*, 14831–14837.

(57) Capobianco, A.; Borrelli, R.; Noce, C.; Peluso, A. Franck-Condon Factors in Curvilinear Coordinates: The Photoelectron Spectrum of Ammonia. *Theor. Chem. Acc.* **2012**, *131*, 1181.

(58) Borrelli, R.; Di Donato, M.; Peluso, A. Quantum Dynamics of Electron Transfer from Bacteriochlorophyll to Pheophytin in Bacterial Reaction Centers. *J. Chem. Theory Comput.* **2007**, *3*, 673–680.

(59) Borrelli, R.; Peluso, A. MolFC: A program for Franck-Condon integrals calculation. Package available online at `http://www.theochem.unisa.it`.

(60) von Niessen, W. Density Localization of Atomic and Molecular Orbitals II. Homonuclear Diatomic Molecules. *Theor. Chim. Acta* **1972**, *27*, 9–23.

(61) Capobianco, A.; Borrelli, R.; Landi, A.; Velardo, A.; Peluso, A. Absorption Band Shapes of a Push-Pull Dye Approaching the Cyanine Limit: A Challenging Case for First Principle Calculations. *J. Phys. Chem. A* **2016**, *120*, 5581–5589.

(62) Yanai, T.; Tew, D. P.; Handy, N. C. A New Hybrid Exchange-Correlation Functional Using the Coulomb-Attenuating Method (CAM-B3LYP). *Chem. Phys. Lett.* **2004**, *393*, 51–57.

(63) Capobianco, A.; Centore, R.; Noce, C.; Peluso, A. Molecular Hyperpolarizabilities of Push-Pull Chromophores: A Comparison between Theoretical and Experimental Results. *Chem. Phys.* **2013**, *411*, 11–16.

(64) Dilling, W. L. The Effect of Solvent on the Electronic Transitions of Benzophenone and Its o- and p-Hydroxy Derivatives. *J. Org. Chem.* **1966**, *31*, 1045–1050.

(65) Kamei, S.; Sato, T.; Mikami, N.; Ito, M. n, π^* State of Jet-Cooled Benzophenone As Studied by Sensitized Phosphorescence Excitation Spectroscopy. *J. Phys. Chem.* **1986**, *90*, 5615–5619.

(66) Sergentu, D.-C.; Maurice, R.; Havenith, R. W. A.; Broer, R.; Roca-Sanjuán, D. Computational determination of the dominant triplet population mechanism in photoexcited benzophenone. *Phys. Chem. Chem. Phys.* **2014**, *16*, 25393–25403.

(67) El-Sayed, M. A. The Triplet state. Its radiative and nonradiative properties. *Acc. Chem. Res.* **1968**, *1*, 8–16.

(68) Borrelli, R.; Di Donato, M.; Peluso, A. Role of Intramolecular Vibrations in Long-range Electron Transfer between Pheophytin and Ubiquinone in Bacterial Photosynthetic Reaction Centers. *Biophys. J.* **2005**, *89*, 830–841.

(69) Ohmori, N.; Suzuki, T.; Ito, M. Why does intersystem crossing occur in isolated molecules of benzaldehyde, acetophenone, and benzophenone? *J. Phys. Chem.* **1988**, *92*, 1086–1093.

(70) Berger, R.; Fischer, C.; Klessinger, M. Calculation of the Vibronic Fine Structure in Electronic Spectra at Higher Temperatures. 1. Benzene and Pyrazine. *J. Phys. Chem. A* **1998**, *102*, 7157–7167.

(71) Improta, R.; Barone, V.; Santoro, F. Ab Initio Calculations of Absorption Spectra of Large Molecules in Solution: Coumarin C153. *Angew. Chem. Int. Ed.* **2007**, *46*, 405–408.

(72) Kusinski, M.; Nagesh, J.; Gladkikh, M.; Izmaylov, A. F.; Jockusch, R. A. Deuterium isotope effect in fluorescence of gaseous oxazine dyes. *Phys. Chem. Chem. Phys.* **2019**, *21*, 5759–5770.

(73) Simpson, J. D.; Offen, H. W. Pressure Dependence of Benzophenone Phosphorescence. *J. Chem. Phys.* **1970**, *52*, 1467.

(74) Borkman, R. F.; Kearns, D. R. Heavy-Atom and Substituent Effects on S-T Transitions of Halogenated Carbonyl Compounds. *J. Chem. Phys.* **1967**, *46*, 2333–2341.

(75) Kresin, V. Z.; Lester, W. A. On the Mechanism of Singlet-Triplet Transitions. *Chem. Phys. Lett.* **1987**, *138*, 59–64.

(76) Kubo, R.; Toyozawa, Y. Application of the Method of Generating Function to Radiative and Non-Radiative Transitions of a Trapped Electron in a Crystal. *Prog. Theor. Phys.* **1955**, *13*, 160–182.

(77) Borrelli, R.; Peluso, A. The Temperature Dependence of Radiationless Transition Rates from Ab Initio Computations. *Phys. Chem. Chem. Phys.* **2011**, *13*, 4420–4426.

(78) Husimi, K. Some Formal Properties of the Density Matrix. *Proc. Phys.-Math. Soc. Jpn.* **1940**, *22*, 264–314.

(79) Borrelli, R.; Capobianco, A.; Peluso, A. Generating Function Approach to the Calculation of Spectral Band Shapes of Free-Base Chlorin Including Duschinsky and Herzberg-Teller Effects. *J. Phys. Chem. A* **2012**, *116*, 9934–9940.
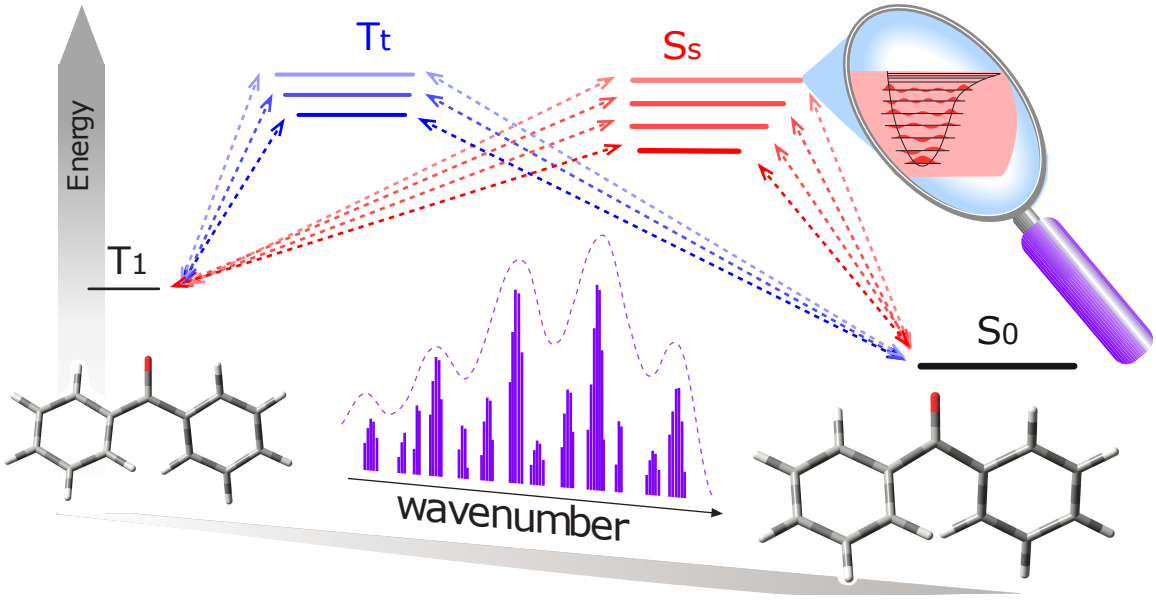
Graphical TOC